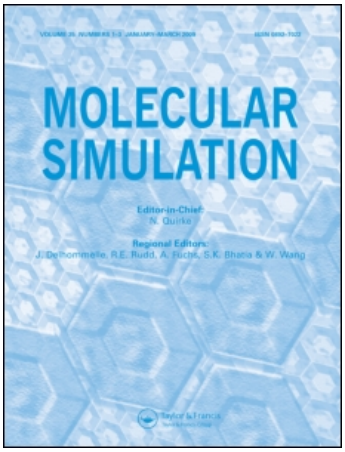

Molecular Simulation

Publication details, including instructions for authors and subscription information:
http://www.informaworld.com/smpp/title~content=t713644482

Pore-scale modeling of non-isothermal reaction phenomena in digitally reconstructed porous catalyst

P. Kočí[a]; F. Štěpánek[b]; M. Kubíček[c]; M. Marek[a]

[a] Department of Chemical Engineering, Center for Nonlinear Dynamics of Chemical and Biological Systems, Institute of Chemical Technology, Prague, Prague, Czech Republic [b] Department of Chemical Engineering, Imperial College London, London, United Kingdom [c] Department of Mathematics, Center for Nonlinear Dynamics of Chemical and Biological Systems, Institute of Chemical Technology, Prague, Prague, Czech Republic

To cite this Article Kočí, P. , Štěpánek, F. , Kubíček, M. and Marek, M.(2007) 'Pore-scale modeling of non-isothermal reaction phenomena in digitally reconstructed porous catalyst', Molecular Simulation, 33: 4, 369 — 377
To link to this Article: DOI: 10.1080/08927020601156426
URL: http://dx.doi.org/10.1080/08927020601156426

Molecular Simulation, Vol. 33, Nos. 4–5, 15–30 April 2007, 369–377

Pore-scale modeling of non-isothermal reaction phenomena in digitally reconstructed porous catalyst

P. KOČÍ†*, F. ŠTĚPÁNEK‡§, M. KUBÍČEK¶‖ and M. MAREK†#

†Department of Chemical Engineering, Center for Nonlinear Dynamics of Chemical and Biological Systems, Institute of Chemical Technology, Prague, Technická 5, 166 28 Prague, Czech Republic
‡Department of Chemical Engineering, Imperial College London, Prince Consort Road, SW7 2AZ London, United Kingdom
¶Department of Mathematics, Center for Nonlinear Dynamics of Chemical and Biological Systems, Institute of Chemical Technology, Prague, Technická 5, 166 28 Prague, Czech Republic

(Received June 2006; in final form November 2006)

Meso-scale mathematical model of local reaction and transport processes in a porous, supported heterogeneous catalyst with bimodal pore-size distribution is presented. The model takes into account individual reaction steps on active sites (microkinetics), diffusion of reactants in macro-pores and meso-/micro-pores (molecular and Knudsen-diffusion), and heat generation and transport. The processes are modelled within a three-dimensional domain ($\approx 10 \times 10 \times 10\,\mu m^3$) of computer-reconstructed porous catalyst. The methodology is demonstrated on CO oxidation on Pt/γ-Al_2O_3. Several 3D porous structures are digitally reconstructed by the methods of particle packing and Gaussian-correlated random fields from typical electron-microscopy images of the catalyst. Typical dependences of overall reaction rate and effectiveness factor on the temperature and properties of the porous catalyst structure are evaluated. Relative importance of diffusion in macro- and meso-pores under varying temperature is demonstrated. Local optimum of effectiveness factor is found for the mixing ratio of catalyst support particles with two different sizes. The resulting temperature gradients over the studied section of catalyst are very small (approximately 0.2 K for the CO concentrations in the order of 1% mol). The results represent the local situation on the meso-scale, which can be interpreted as one discretisation point in the full-scale model of the reactor.

Keywords: Meso-scale modeling; Porous structure; Reaction and transport; CO oxidation; Pt/γ-Al_2O_3 catalyst

1. Introduction

Multi-scale simulation in heterogeneous catalysis is emerging, cf. [1]. Information on a finer scale is computed and passed to a model at a larger (coarser) scale. The main goal is to predict the macroscopic behaviour of an engineering system from first principles (up-scaling or bottom–up approach). For example, the processes on the following levels have to be considered in a typical monolith reactor used for car exhaust treatment (in orders of scale): monolith length and diameter ≈ 10 cm, channel diameter ≈ 1 mm, the porous catalytic layer ≈ 10–$100\,\mu$m, the catalyst support micro-particles diameter $\approx 1-10\,\mu$m, macro-pores diameter ≈ 100 nm$-1\,\mu$m, meso-/micro-pores diameter $\approx 1-10$ nm, the catalytically-active metal crystallites $\approx 1-10$ nm, and the reacting molecules $\approx$ Ångströms. This leads to a typical multi-scale problem [1].

Detailed information about the porous structure of a supported heterogeneous catalyst (pore-size distribution, typical sizes of particles, etc.) on the micro- and nano-scale levels can be obtained from scanning electron microscopy (SEM), transmission electron microscopy (TEM) or other high-resolution imaging techniques [1–3]. This information can be used in the computer reconstruction of porous catalytic medium [1]. The reconstruction can be either stochastic, based on the evaluated porosity and the correlation function of the porous medium [4], or semi-deterministic, based on the approximate simulation of the actual process of formation of the porous medium (e.g. agglomeration of particles [5], drying, impregnation, calcination). In the digitally-reconstructed porous med-

*Corresponding author. Tel.: + 420-22044-3293. Fax: + 420-22044-4320. Email: petr.koci@vscht.cz
§Email: f.stepanek@ic.ac.uk
‖Email: milan.kubicek@vscht.cz
#Email: milos.marek@vscht.cz, http://www.vscht.cz/monolith

Molecular Simulation
ISSN 0892-7022 print/ISSN 1029-0435 online © 2007 Taylor & Francis
http://www.tandf.co.uk/journals
DOI: 10.1080/08927020601156426

ium, transport (diffusion, permeation, heat conduction [6]), adsorption [7], reaction and combined reaction-diffusion processes [8] can be simulated. Significant advances have been made in the development of models and simulation methods for reaction, transport and transformation processes in porous structures, cf. e.g. [1,3,9,10]. Currently, computer-aided catalyst design and optimisation of porous structures are of increasing importance in both research and industry. The results of parametric studies can then serve as a feedback for the catalyst development.

Catalytic reactions in porous, supported catalyst take place on the active sites (metal crystallites) located on the surface of macro-pores and in the meso-pores of supporting material, simultaneously with mass and heat transport [2,3]. The transport inside the meso-porous particles is usually dominated by Knudsen diffusion, while the transport in the macro-pores can be described by volume (molecular) diffusion. The combined effects of transport and reaction in the porous catalytic layer play an important role in the operation of catalytic reactor. For example, in the monolith converters of automotive exhaust gases the transport limitations influence the light-off temperature, reactor dynamics and overall conversions to a large extent [11–14]. Actual degree of utilisation of the noble metal micro-crystallites can vary. Since the amount of noble metals significantly influences the cost of the reactor, it is desirable to design the catalytic layer in such a way that the utilisation of the active sites is maximised. The structure of the porous catalyst layer (porosity, distribution of pore-sizes, etc.) is usually controlled in the course of catalyst preparation on the two levels: (i) the level of macro-porous structure, influenced, e.g. by mixing of supporting particles with different sizes [1], and (ii) the level of meso-porous structure, determined by the use of specific material of supporting particles (e.g. alumina, silica or zeolites) with the defined meso-porous structure [10].

In the recent paper the first results of meso-scale modeling of CO oxidation in digitally-reconstructed porous Pt/γ-Al_2O_3 catalyst were presented [15]. Simplified situation, describing isothermal reaction system and constant gas component concentrations in the macro-pores was considered. In this contribution, we present more detailed model of reaction-transport processes in porous catalyst, where both possible reaction heat effects (temperature gradients) and diffusion-controlled variable concentrations in macro-pores are considered. The aim is to develop an effective computational methodology for the study of a functional relationship between the micro-structure of the porous layer and the resulting local effectiveness factor under various operating conditions, which can help in the optimisation of the catalyst structure.

2. Computer reconstruction of porous catalyst

The process of porous catalyst reconstruction starts from the evaluation of macro-porosity ε^{M}, sizes of supporting material particles and the correlation function (describing the macro-pore size distribution) [1] from the SEM images of porous catalyst (figure 1). The micro-porosity ε^{μ}, mean meso-/micro-pore diameter d^{μ} of the catalyst support material and sizes of metal crystallites can be estimated from high resolution TEM images. The estimated values are then confronted with the data obtained from mercury porosimetry and adsorption/desorption isotherms.

The computer-reconstructed medium is represented by a volume phase function in the form of 3D matrix and it exhibits the same characteristics (porosity, correlation length, characteristic size of macro-pores) as the original porous catalyst [1]. The 3D matrix contains the information about the phase in each discretisation point (voxel), i.e. the presence of either gas (macro-pore) or meso-porous supporting material.

The reconstruction can be either stochastic or semi-deterministic. The method of Gaussian-correlated random fields [16] is representative of the former case, while close random packing (ballistic deposition) of particles followed by partial sintering [5] corresponds to the latter case. Both cases represent the simplest structural models

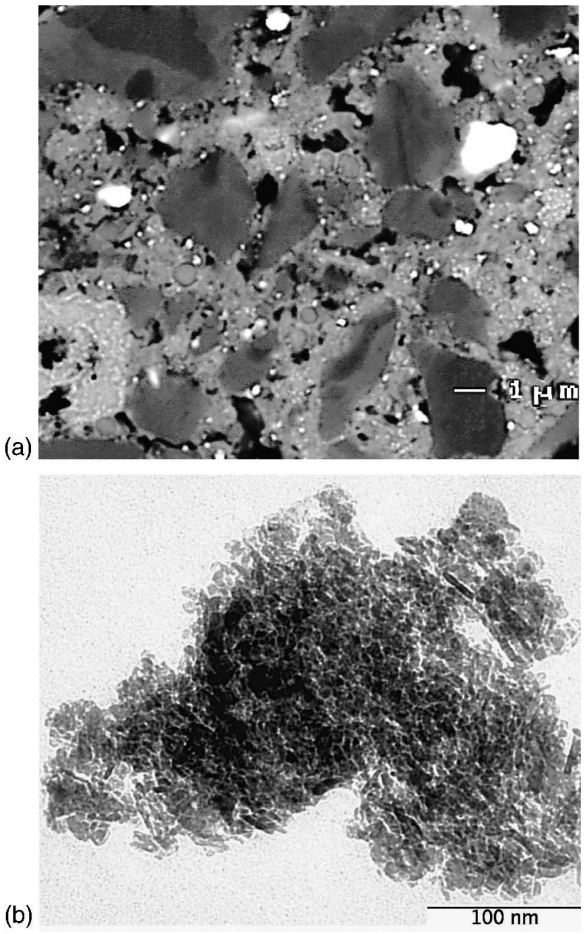

Figure 1. (a) SEM image of porous Pt/CeO_2/γ-Al_2O_3 catalyst. Black, macro-pores, grey, meso-porous γ-Al_2O_3 with dispersed Pt, white, meso-porous CeO_2. ε^{M} evaluated from more SEM images is approx. 15%. (b) TEM image of meso-porous γ-Al_2O_3 with dispersed Pt. Courtesy of Ecocat Oy.

of porous media, possessing the basic qualitative features of real porous media [1]. Two input parameters are used in the case of Gaussian-correlated media—the macro-porosity ε^{M} and the pore-space correlation length L_{xy}, related to the mean hydraulic diameter of macro-pores $d_{\mathrm{h}}^{\mathrm{M}}$. The packing of bi-disperse particles is then specified by four parameters: the radii of large and small particles, their mixing ratio, and the fractional overlap between the particles (typically 0.15–0.20).

Examples of porous media generated by packing of particles are given in figures 2 and 3(a),(b), the example of stochastic Gaussian porous medium is depicted in figure 3(c).

The characteristic macro-pore size can be expressed by the correlation length L_{xy} or as the mean hydraulic diameter $d_{\mathrm{h}}^{\mathrm{M}}$:

$$d_{\mathrm{h}}^{\mathrm{M}} = 4\frac{V^{\mathrm{M}}}{S^{\mathrm{M}}} \tag{1}$$

Here V^{M} and S^{M} are the volume and surface area of the macro-pores, respectively. The macroporosity ε^{M} is defined as:

$$\varepsilon^{\mathrm{M}} = \frac{V^{\mathrm{M}}}{V^{\mathrm{w}}}, \tag{2}$$

where V^{w} is total volume of the studied section of porous medium. The density of macro-pores surface area (a^{M}) is calculated from:

$$a^{\mathrm{M}} = \frac{S^{\mathrm{M}}}{V^{\mathrm{w}}}, \tag{3}$$

The characteristics of several reconstructed porous catalysts used in the simulations are summarised in table 1.

3. Modeling of reactions and transport

3.1 Mass transport

If the gas concentrations of reactants and products are low, mass transport can be approximated by the Fick's law. Spatially 3D distributed reaction-diffusion problem in a porous catalyst is then described by mass balances in the form of the following partial differential equations (4) and (5).

For gas components $k = 1 \ldots K$:

$$\varepsilon^{\mu}\frac{\partial cY_k(x,y,z,t)}{\partial t} = D_k^{\mathrm{eff}} c\left(\frac{\partial^2 Y_k}{\partial x^2} + \frac{\partial^2 Y_k}{\partial y^2} + \frac{\partial^2 Y_k}{\partial z^2}\right) + \sum_{j=1}^{J} \nu_{k,j} \cdot r_j \tag{4}$$

For surface-deposited components $i = 1 \ldots I$:

$$\frac{\partial \theta_i(x,y,z,t)}{\partial t} = \frac{1}{C_{\mathrm{Pt}}} \sum_{j=1}^{J} \nu_{i,j} \cdot r_j \tag{5}$$

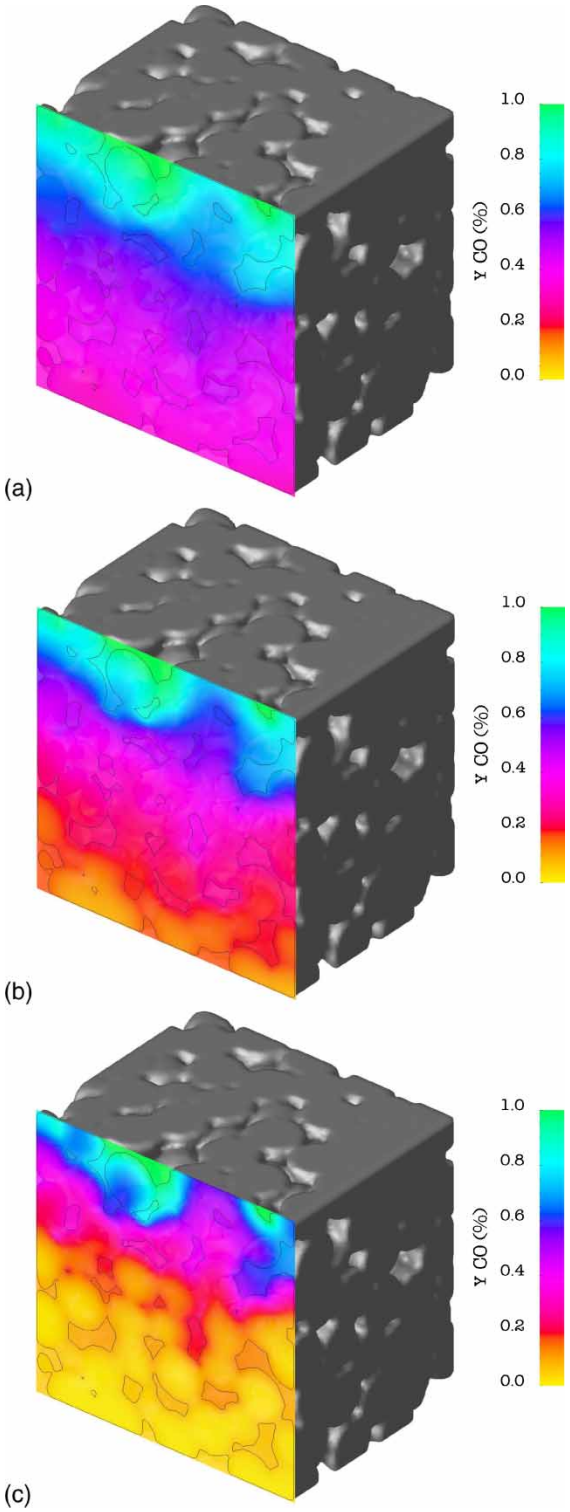

Figure 2. Effect of temperature on the reactant (CO) concentration in the porous Pt/γ-Al_2O_3 catalyst reconstructed by particle-packing method. γ-Al_2O_3 particles diameter 2 μm, $d_{\mathrm{h}}^{\mathrm{M}} = 310$ nm, $\varepsilon^{\mathrm{M}} = 16.0\%$. Free space corresponds to macro-pores, solid grey corresponds to meso-porous γ-Al_2O_3 with dispersed Pt. Length of the section edge 10 μm, coordinate z_1 is at the top. (a) $T^{\mathrm{bnd}} = 473$ K, (b) $T^{\mathrm{bnd}} = 493$ K, (c) $T^{\mathrm{bnd}} = 513$ K.

Here x, y and z are spatial coordinates in the porous catalyst, Y_k denotes local molar fraction of the k-th gas component, c is total molar gas concentration ($c = p/(R^{\mathrm{g}}T)$ for ideal gas), θ_i is local coverage of active catalytic sites

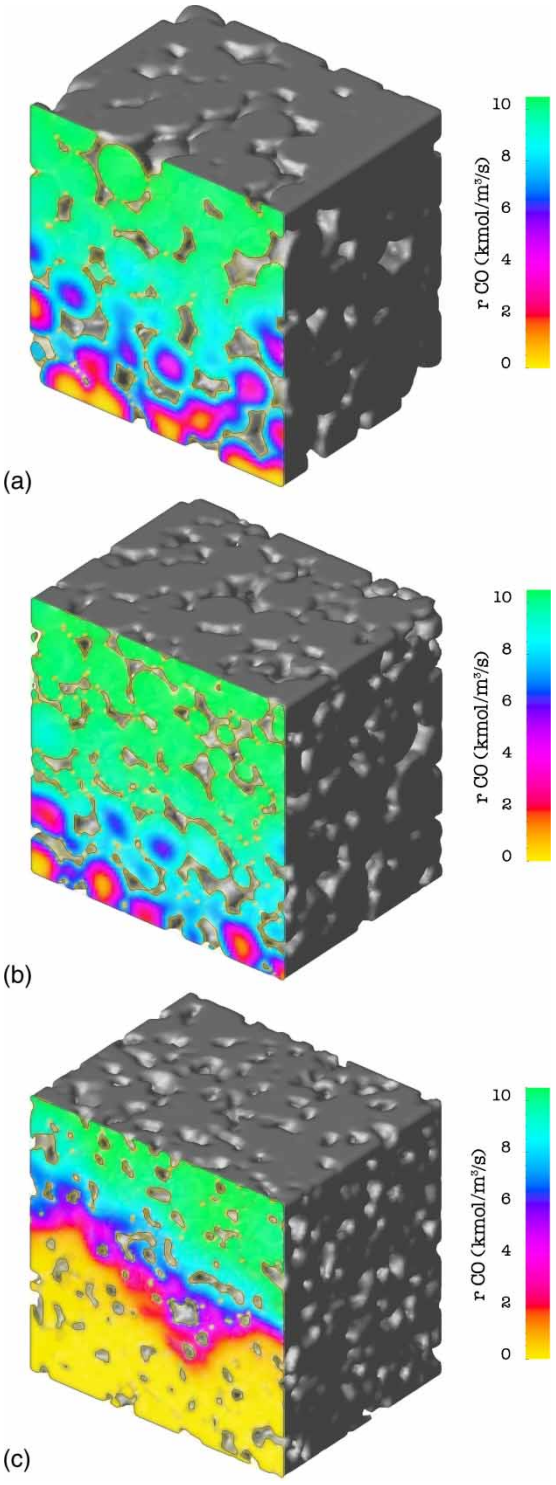

Figure 3. Reaction rate profiles (r_{CO}) in the Pt/γ-Al_2O_3 catalysts with different porous structures, generated by particle packing (a), (b) and by the stochastic method of correlated Gaussian fields (c). Free space corresponds to macro-pores, solid grey corresponds to meso-porous γ-Al_2O_3 with dispersed Pt, $T^{bnd} = 513$ K. Length of the section edge 10 μm, coordinate z_1 is at the top. (a) γ-Al_2O_3 particles diameter 2 μm, $d_h^M = 310$ nm, $\varepsilon^M = 16.0\%$. (b) γ-Al_2O_3 particles diameter 2 and 1 μm in ratio 1:4, $d_h^M = 240$ nm, $\varepsilon^M = 17.3\%$. (c) Stochastic, $d_h^M = 230$ nm, $\varepsilon^M = 15.0\%$.

by the i-th surface component, C_{Pt} is local concentration of active catalytic sites, $\nu_{k,j}$ is stoichiometric coefficient of the component k in the j-th reaction step, r_j is local reaction rate of the j-th reaction step, D_k^{eff} is local effective diffusivity of the k-th component, and ε^μ is local microporosity ($\varepsilon^\mu = 1$ in the macro-pores).

Table 1. Properties of the reconstructed-porous catalysts.

Catalyst	*Macro-pore hydraulic diameter* d_h^M (nm)	*Density of macro-pores surface area* a^M ($m^2\,m^{-3}$)	*Macroporosity* ε^M
Packed 1:0	310	1.10×10^7	16.0
Packed 1:1	275	1.24×10^7	16.0
Packed 1:4	240	1.50×10^7	17.3
Packed 1:8	220	1.62×10^7	17.4
Packed 1:16	200	1.91×10^7	16.8
Gaussian 1	230	1.55×10^7	15.0
Gaussian 2	325	0.99×10^7	15.0

"Packed", catalyst generated by packing of γ-Al_2O_3 particles with diameters 2 and 1 μm in the given ratio; "Gaussian", catalyst generated by the stochastic method of Gaussian-correlated random fields.

The given set of partial differential equations is solved within the spatially 3D section of porous catalyst ($x \in < x_0, x_1 >$, $y \in < y_0, y_1 >$, $z \in < z_0, z_1 >$). After equidistant spatial discretisation of the domain with the step h into N_x, N_y, N_z volume elements (corresponding to voxels of digitally-reconstructed porous catalyst), the distributed system variables can be represented by 3D matrices. Using discretisation indices $m = 1 \ldots N_x$, $n = 1 \ldots N_y$ and $o = 1 \ldots N_z$ in the directions x, y and z, respectively, the balances (4) for gas components $k = 1 \ldots K$ become:

$$
\begin{aligned}
&\varepsilon^{\mu,m,n,o} \frac{\mathrm{d}c^{m,n,o} Y_k^{m,n,o}}{\mathrm{d}t} \\
&= \bar{D}_k^{<m-1,m>,n,o} \bar{c}^{<m-1,m>,n,o} \frac{Y_k^{m-1,n,o} - Y_k^{m,n,o}}{h^2} \\
&\quad + \bar{D}_k^{<m+1,m>,n,o} \bar{c}^{<m+1,m>,n,o} \frac{Y_k^{m+1,n,o} - Y_k^{m,n,o}}{h^2} \\
&\quad + \bar{D}_k^{m,<n-1,n>,o} \bar{c}^{m,<n-1,n>,o} \frac{Y_k^{m,n-1,o} - Y_k^{m,n,o}}{h^2} \\
&\quad + \bar{D}_k^{m,<n+1,n>,o} \bar{c}^{m,<n+1,n>,o} \frac{Y_k^{m,n+1,o} - Y_k^{m,n,o}}{h^2} \\
&\quad + \bar{D}_k^{m,n,<o-1,o>} \bar{c}^{m,n,<o-1,o>} \frac{Y_k^{m,n,o-1} - Y_k^{m,n,o}}{h^2} \\
&\quad + \bar{D}_k^{m,n,<o+1,o>} \bar{c}^{m,n,<o+1,o>} \frac{Y_k^{m,n,o+1} - Y_k^{m,n,o}}{h^2} \\
&\quad + \sum_{j=1}^{J} \nu_{k,j} r_j^{m,n,o}
\end{aligned}
\tag{6}
$$

The spatially discrete form of equation (5) is obtained in a similar way. In the steady state $\partial c Y_k / \partial t = 0$ and $\partial \theta_i / \partial t = 0$. Then (after the spatial discretisation) a large set of algebraic equations is obtained ($N_x \times N_y \times N_z \times$

$(K + I)$ equations). The resulting set of equations is then solved iteratively by the Gauss–Seidel method.

The $\bar{D}_k^{<m-1,m>,n,o}$ in equation (6) denotes mean effective diffusion coefficient of the component k between two adjacent volume elements with the coordinates $(m-1, n, o)$ and (m, n, o); similarly for other combinations of the spatial indices m, n, o:

$$\bar{D}_k^{<m-1,m>,n,o} = \frac{2D_k^{\text{eff},m-1,n,o} \cdot D_k^{\text{eff},m,n,o}}{D_k^{\text{eff},m-1,n,o} + D_k^{\text{eff},m,n,o}} \tag{7}$$

The $\bar{c}^{<m-1,m>,n,o}$ in equation (6) is mean molar gas concentration between two adjacent volume elements with the coordinates $(m-1, n, o)$ and (m, n, o); similarly for other combinations of the spatial indices m, n, o:

$$\bar{c}^{<m-1,m>,n,o} = \frac{c^{m-1,n,o} + c^{m,n,o}}{2} \tag{8}$$

The local values of effective diffusivity D_k^{eff} in the meso-pores are calculated from the equation for Knudsen-diffusion coefficient:

$$D_k^{\text{eff}} = \frac{\varepsilon^{\mu}}{\tau^{\mu}} \frac{d^{\mu}}{3} \sqrt{\frac{8R^{\text{g}}T}{W_k \pi}} \tag{9}$$

Here ε^{μ} and τ^{μ} denote the local microporosity and tortuosity of mesoporous support material, respectively, W_k is the molar weight of the component k, and d^{μ} is the mean transport meso-pore diameter.

In the macro-pores, the following correlation for volume diffusivity of the component k in the reference gas "ref" (pseudo-component representing the complete gas mixture) can be used [17]:

$$D_k^{\text{eff}} = \frac{144.9\, T^{1.75}/p}{\sqrt{2/(10^{-3}/W_k + 10^{-3}/W_{\text{ref}})}\left(\omega_k^{1/3} + \omega_{\text{ref}}^{1/3}\right)^2} \tag{10}$$

Here ω_k is the volume diffusion constant of the gas component k and p is total pressure.

Measured values of overall effective diffusivities in typical γ-Al_2O_3-based porous catalyst layer used in monolith converters of automobile exhaust gases vary from 1×10^{-7} to $1\times10^{-6}\,\text{m}^2\,\text{s}^{-1}$, depending on actual porous structure [18].

3.2 Heat transport

Possible evolution of temperature gradients (non-isothermal effects) over the studied catalyst section are described on the meso-scale by the following enthalpy balance:

$$\rho^{\text{eff}} c_p^{\text{eff}} \frac{\partial T(x,y,z,t)}{\partial t} = \lambda^{\text{eff}} \left(\frac{\partial^2 T}{\partial x^2} + \frac{\partial^2 T}{\partial y^2} + \frac{\partial^2 T}{\partial z^2}\right) + \sum_{j=1}^{J} -\Delta H_{r,j} \cdot r_j \tag{11}$$

Here λ^{eff}, ρ^{eff} and $c_{\text{p}}^{\text{eff}}$ are local effective heat conductivity, density and heat capacity, respectively, T is local temperature, and $\Delta H_{r,j}$ is standard reaction enthalpy of the j-th reaction step. The enthalpy balance (11) can be transformed into spatially discrete form and then solved in the same way as described for the mass balance (4). Local mean heat conductivity values ($\overline{\lambda^{\text{eff}}}$) are used in analogy to local mean diffusivities ($\bar{D}_k$), cf. equations (6) and (7).

3.3 Boundary conditions

Different types of boundary conditions can be defined in the studied section of porous catalyst to account for different system configurations. The most usual boundary conditions are: (i) constant boundary value, used on the boundaries with significant mass or heat exchange with the surroundings (12) and (13), and (ii) zero flux across the boundary (14)–(16). The other possibilities include periodic boundary conditions and the conditions of constant flux. In this paper the following configuration is used:

$$Y_k|_{z=z_1} = Y_k^{\text{bnd}} \text{ (in macropores only)} \tag{12}$$

$$T|_{z=z_1} = T^{\text{bnd}} \tag{13}$$

$$\left.\frac{\partial Y_k}{\partial x}\right|_{x=x_0,x_1} = 0, \quad \left.\frac{\partial Y_k}{\partial y}\right|_{y=y_0,y_1} = 0, \quad \left.\frac{\partial Y_k}{\partial z}\right|_{z=z_0} = 0 \tag{14}$$

$$\left.\frac{\partial Y_k}{\partial z}\right|_{z=z_1} = 0 \text{ (in mesopores only)} \tag{15}$$

$$\left.\frac{\partial T}{\partial x}\right|_{x=x_0,x_1} = 0, \quad \left.\frac{\partial T}{\partial y}\right|_{y=y_0,y_1} = 0, \quad \left.\frac{\partial T}{\partial z}\right|_{z=z_0} = 0 \tag{16}$$

These boundary conditions correspond to the local situation in a catalyst layer with the slab geometry, where the source flux of gaseous reactants is via macro-pores at the boundary z_1, with dominant heat and mass transport in the direction z (cf. e.g. figure 2). The Y_k^{bnd} and T^{bnd} are chosen boundary values of components molar fractions and temperature, respectively.

3.4 Reactions

Catalytic reactions take place on the active sites (metal crystallites) located on the surface of macro-pores and in the meso-pores of supporting material. Local reaction rate depends on the local concentrations of gas reactants, surface-deposited intermediates, concentration of active sites, and temperature [2]. Rate constant k_j of the j-th reaction step is an exponential function of temperature ($k_{0,j}$ denotes the pre-exponential factor, $E_{\text{a},j}$ is the activation energy, R^{g} is the universal gas constant):

$$k_j = k_{0,j} \exp\left(-\frac{E_{\text{a},j}}{R^{\text{g}}T}\right) \tag{17}$$

The effectiveness factor η_j over the studied section of catalyst is defined as:

$$\eta_j = \frac{1}{V^s \cdot r_j^{\mathrm{surf}}} \int_{V^s} r_j \, \mathrm{d}V, \tag{18}$$

where r_j^{surf} is the reaction rate of the j-th step at the conditions occurring on external catalyst surface (boundary value).

Catalytic oxidation of CO on Pt/γ-Al_2O_3 have been chosen as a model reaction system for the demonstration of the presented methodology. This reaction takes place in catalytic monolith converters used for automotive exhaust after treatment as well as in other applications of catalysis [2,19,20]. Crystallites of noble metals (typically Pt, Rh and/or Pd) are dispersed on the γ-Al_2O_3 support as active catalytic components. Other compounds are often added to the washcoat to stabilise the porous structure; they may also act as active catalytic centres (e.g. CeO_2—ZrO_2) [21]. Characteristic meso-pore diameter of γ-Al_2O_3 support particles is approximately 10 nm, while the macro-porous structure depends on the actual catalyst preparation process (macro-pores diameter is usually 100 nm^{-1} μm).

The reaction steps considered in CO oxidation mechanism are listed in table 2. The values of respective kinetic parameters $k_{0,j}$ and $E_{\mathrm{a},j}$ (evaluated from transient reaction experiments [22,23]) are given in table 3. The reaction scheme in table 2 represents basic Langmuir–Hinshelwood mechanism, which forms a sub-model of the more complex scheme for CO oxidation on Pt(Rh)/CeO_2/γ-Al_2O_3 catalyst, where catalytic effects of the added CeO_2 are also quantified [22,23].

Non-linear dynamic phenomena including stable oscillations and multiplicity of steady states have been described for more complex CO oxidation scheme in certain range of operating conditions [13]. However, no such behaviour has been observed in the simplified CO oxidation model used here.

In the following text the symbols r_{CO} or r without a subscript denote the value of net CO reaction rate (note that in steady state $r_1 = r_2/2 = r_3$ in table 2):

$$r = r_{\mathrm{CO}} = -\nu_{\mathrm{CO},1} \cdot r_1 \tag{19}$$

Similarly, the effectiveness factor η with no subscript is related to the net CO reaction rate r_{CO}.

Table 2. Microkinetic reaction scheme used in the model.

Number	*Reaction step*	*Kinetic expression*
1	$\mathrm{CO} + * \rightleftarrows \mathrm{CO}^*$	$r_1 = k_1^{\mathrm{f}} C_{\mathrm{Pt}} c_{\mathrm{CO}} \theta_* - k_1^{\mathrm{b}} C_{\mathrm{Pt}} \theta_{\mathrm{CO}^*}$
2	$\mathrm{O}_2 + 2* \rightarrow 2\mathrm{O}^*$	$r_2 = k_2 C_{\mathrm{Pt}} c_{\mathrm{O}_2} \theta_*$
3	$\mathrm{CO}^* + \mathrm{O}^* \rightarrow \mathrm{CO}_2 + 2*$	$r_3 = k_3 C_{\mathrm{Pt}} \theta_{\mathrm{CO}^*} \theta_{\mathrm{O}^*}$

Asterisk (*) denotes noble metal sites, $c_k = cY_k$. For more details about the reaction scheme and values of the kinetic parameters cf. [22,23].

Table 3. The values of model parameters.

Parameter	*Value*
ε^{M}	5–25%
d^{μ}	11 nm
ε^{μ}	0.7
τ^{μ}	10
$d_{\mathrm{h}}^{\mathrm{M}}$	200–500 nm
$N_x \times N_y \times N_z$	85 × 85 × 85
h	118 nm
$Y_{\mathrm{CO}}^{\mathrm{bnd}}$	1.0% mol
$Y_{\mathrm{O}_2}^{\mathrm{bnd}}$	0.5% mol
C_{Pt}	50 mol m^{-3}
$\lambda^{\mathrm{eff,s}}$	0.5 $\mathrm{Wm}^{-1}\,\mathrm{K}^{-1}$
$\lambda^{\mathrm{eff,g}}$	0.04 $\mathrm{Wm}^{-1}\,\mathrm{K}^{-1}$
$(\rho c_{\mathrm{p}})^{\mathrm{eff,s}}$	10^6 J $\mathrm{m}^{-3}\,\mathrm{K}^{-1}$
$(\rho c_{\mathrm{p}})^{\mathrm{eff,g}}$	645 J $\mathrm{m}^{-3}\,\mathrm{K}^{-1}$
Reference gas	N_2
T^{bnd}	433–533 K
p	101,325 Pa
$k_{0,1}^{\mathrm{f}}$	9.00 × 10^5
$E_{\mathrm{a},1}^{\mathrm{f}}$	0 J $\mathrm{mol}^{-1}\,\mathrm{K}^{-1}$
$k_{0,1}^{\mathrm{b}}$	5.65 × 10^{14}
$E_{\mathrm{a},1}^{\mathrm{b}}$	113,000 J $\mathrm{mol}^{-1}\,\mathrm{K}^{-1}$
$k_{0,2}$	1.01 × 10^5
$E_{\mathrm{a},2}$	0 J $\mathrm{mol}^{-1}\,\mathrm{K}^{-1}$
$k_{0,3}$	2.81 × 10^{13}
$E_{\mathrm{a},3}$	96,800 J $\mathrm{mol}^{-1}\,\mathrm{K}^{-1}$

For more details about the values of reaction kinetic parameters cf. [22,23].

4. Results and discussion

Series of simulations were performed to demonstrate the presented methodology and to study the effects of temperature and catalyst structure on the overall reaction rate and effectiveness factor. The values of model parameters used in the simulations are summarised in table 3. The characteristics of the porous structures employed in the simulations are summarised in table 1.

The examples of results obtained for the steady-state CO oxidation in the porous Pt/γ-Al_2O_3 catalyst, digitally reconstructed by the packing of mesoporous γ-Al_2O_3 particles, are given in the figure 2. The occurrence of local concentration gradients reflects the interplay between reaction and transport processes in macro-pores and meso-pores. For the lower temperature (figure 2(a)) a smooth concentration field is established. Local mass transport inside the mesoporous catalyst particles is fast enough in comparison with local reaction rates, so that practically only the dominant gradient in the direction z occurs. The direction of this gradient is determined by the used boundary conditions (12)–(16); here the source of reactants is at $z = z_1$. Both macro- and meso-pores contribute to the transport, however, the diffusion through the macro-pores is much faster—for the parameters given in table 3 typically $D_{\mathrm{CO}}^{\mathrm{eff}}$ in macro-pores is $5{\times}10^{-5}\,\mathrm{m}^2\,\mathrm{s}^{-1}$, while in mesoporous γ-$Al_2O_3$ particles it is approximately $5{\times}10^{-8}\,\mathrm{m}^2\,\mathrm{s}^{-1}$.

In the case of higher temperatures (figure 2(b),(c)) we can observe that steep local concentration gradients can

occur in the system in all spatial directions (x, y, z). Two types of concentration gradients can be recognised: (i) the longer-range concentration gradient in the direction z (dominant gradient over the catalyst section), and (ii) the short-range local gradients within the individual meso-porous catalyst particles. For high temperatures (and thus high reaction rates) there are even regions with practically zero CO concentration (figure 2(c)). The reaction takes place mainly close to the surface of the macro-pores, where the gaseous reactants can be relatively easily transported. The Pt crystallites distributed deeper in the γ-Al_2O_3 meso-pores are not utilised under such conditions.

Examples of the reaction rate profiles inside three different porous catalyst structures are shown in figure 3. The first two catalysts (figure 3(a),(b)) were generated by packing of γ-Al_2O_3 particles in different ratio, while the third catalyst (figure 3(c)) represent the stochastic medium generated by the method of Gaussian-correlated random fields. The differences between individual catalysts can be clearly seen—the highest overall reaction rate is here observed for the structure of particles with two different sizes (figure 3(b)), while the Gaussian (stochastically-generated) catalyst suffers from insufficient transport of the reactants into the lower parts of the porous catalyst (in the spatial direction z). These differences will be discussed in more detail later in this paper.

Typical temperature profile generated within the section of the porous structure is depicted in figure 4. It can be observed that for the present CO concentration and reaction rate the temperature gradients are very small, in the order of 0.1 K over the simulated catalyst section. This result follows from the size of the catalyst domain and the order of magnitude of the γ-Al_2O_3 effective heat conductivity (table 3). The effects of possible local overheating of Pt crystallites in the meso-pores can be described on the nano-scale level. In this paper we have used spatially averaged, pseudo-continuous description of the processes on the catalytic sites, with a characteristic spatial step size ≈ 100 nm (cf. the value of h in table 3). In the studied case it appears that the effects of non-isothermality are not important for the evaluation of effective reaction rate. However, it is possible that after decreasing the step size by several orders of magnitude (to 1 nm level) there could exist local hot spots in the proximity of active catalytic sites.

Examples of the results of parametric studies can be seen in figures 5(a),(b) and 6. Each point on the curves represents the chosen characteristics of the steady-state solution for the CO oxidation in the reconstructed Pt/γ-Al_2O_3 with specific parameters. The influence of temperature and varying porous structure on the effectiveness factor η is depicted in figure 5(a). It is clearly seen that with the increasing temperature (increasing reaction rate) the effectiveness factor sharply decreases and there can exist large differences for different types of porous media. Generally, the resulting effectiveness factors are lower for the porous media generated by the stochastic method of Gaussian-correlated random fields than for the

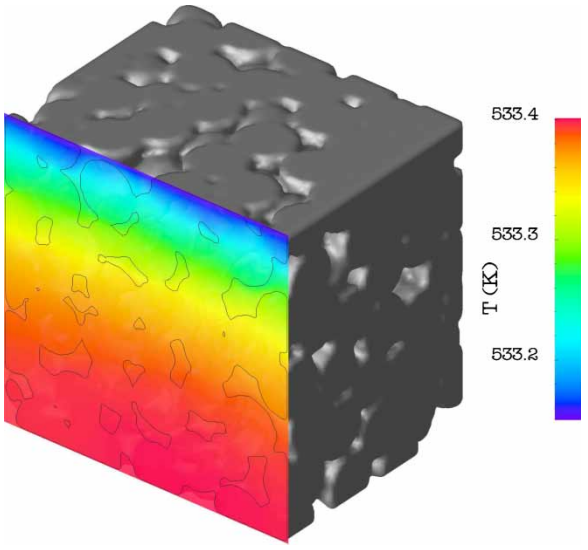

Figure 4. Temperature profile in the porous Pt/γ-Al_2O_3 catalyst reconstructed by particle-packing method. γ-Al_2O_3 particles diameter 2 μm, $d_h^M = 310$ nm, $\varepsilon^M = 16.0\%$. Free space corresponds to macro-pores, solid grey corresponds to meso-porous γ-Al_2O_3 with dispersed Pt. Length of the section edge 10 μm, coordinate z_1 is at the top. Boundary temperature $T^{bnd} = 533.15$ K.

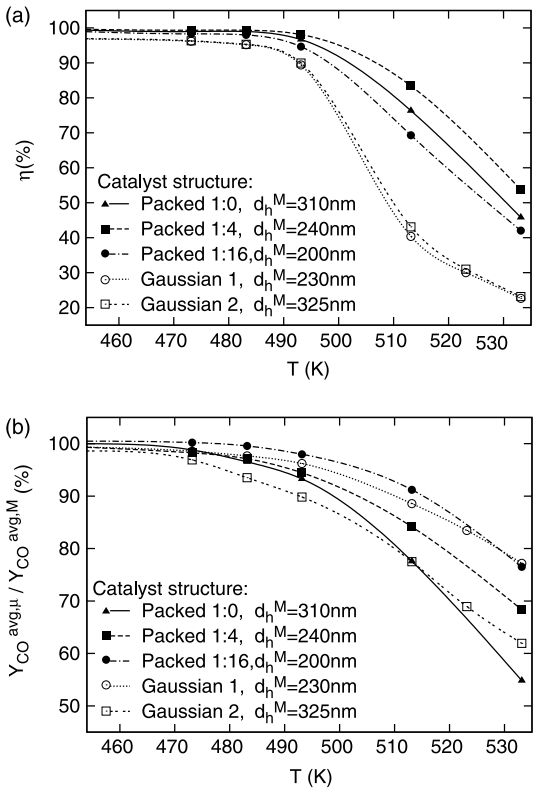

Figure 5. Influence of temperature T and varying catalyst structure on the effectiveness factor η (a) and the ratio of average CO concentrations in macro- and meso-pores $Y_{CO}^{avg,\mu}/Y_{CO}^{avg,M}$ (b) over the studied section of porous catalyst. Legend: "packed", catalyst generated by packing of γ-Al_2O_3 particles with diameters 2 and 1 μm in the given ratio; "gaussian", catalyst generated by the stochastic method of Gaussian-correlated random fields. For the characteristics of individual reconstructed catalysts (cf. table 1).

corresponding structures (similar ε^{M} and d_h^{M}) formed by packed particles. It results form the lower macro-pores connectivity and thus worse overall mass transport properties of the stochastic media. The sudden change in the temperature dependence of the effectiveness factor of Gaussian media between temperatures 490 and 510 K reflects this transport limitation in the macro-pores (compare also the corresponding figure 3).

The effect of diffusion in macro-pores is partly eliminated in figure 5(b), where the ratios of average CO molar fractions in micro- and macro-pores are given ($Y_k^{\mathrm{avg},\mu}/Y_k^{\mathrm{avg,M}}$). This ratio is a measure of local transport limitations on the level of individual meso-porous γ-Al_2O_3 particles. We can see that the temperature dependence of this ratio decreases with the increasing temperature in a similar way for both types of porous media, which reflects the constant meso-porous structure of the supporting material. The differences in effectiveness factor between different porous catalysts are then correlated mainly with the macroporosity and the hydraulic diameter of macro-pores. Such local situation without transport limitations in macro-pores was in more detail studied in Ref. [15].

In figure 6 is then presented the computed dependence of effectiveness factor on the ratio of the small-to-large particles number in the porous structure generated by particle-packing method. The local maximum of η can be observed around the ratio 7:1. When we look at the corresponding characteristics given in table 1 we can conclude that this is the result of interplay between local reaction, transport in macro-pores and transport in meso-pores: (i) The density of macro-pore surface area a^{M} increases with the small-to-large particles ratio, which minimises the local transport limitations, but concurrently (ii) the macro-pores hydraulic diameter d_h^{M} decreases, which makes the transport via macro-pores less efficient. It clearly illustrates that structured porous supports prepared in a controlled way can bring higher catalyst effectiveness.

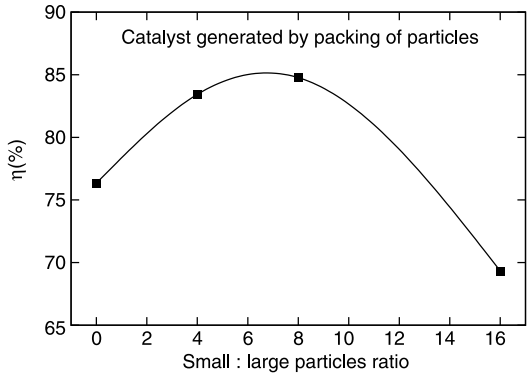

Figure 6. Dependence of the effectiveness factor η on the ratio of small ($d = 1\,\mu$m) and large ($d = 2\,\mu$m) γ-Al_2O_3 particles in the catalyst reconstructed by the particle-packing method. $T = 513$ K, for the characteristics of individual catalysts (cf. table 1).

5. Conclusions

We have presented a methodology for the calculation of the local average reaction rate and local effectiveness factor in a digitally-reconstructed porous catalyst, including the description of individual reaction steps on active sites (microkinetics), diffusion of reactants in macro-pores and meso-/micro-pores (molecular and Knudsen diffusion, respectively), and heat generation and transport. The effectiveness factor has been studied as a function of structural parameters of the porous medium and temperature for the model system of CO oxidation on Pt/γ-Al_2O_3. Non-monotonous dependence of the effectiveness factor on the macro-porosity and hydraulic diameter of the macro-pores has been observed. Local maximum has been found for the mixing ratio of catalyst support particles with two different sizes (1:7 for the particle sizes 2 and 1 μm, respectively). For the used boundary values of CO concentrations on the external catalyst surface ($\approx 1\%$ mol) only small temperature gradients (≈ 0.2 K) are established over the studied section. The results of the parametric studies are useful for better understanding of the reaction-transport effects in porous, supported heterogeneous catalysts and they can serve for the optimisation of the catalyst structure. The methodology presented in this work also contributes to the development of multi-scale simulation techniques whereby volume-averaged parameters calculated at one spatial scale are used as input values for simulations at a larger scale. For example, the calculated dependence of the effectiveness factor on local temperature and boundary concentration in the macro-pores can be used for more accurate simulation at the length-scale of a monolith channel in the important engineering problem—design of a catalytic monolith for treatment of car exhausts.

Acknowledgements

The work has been supported by the grant 104/06/P301 of the Czech Grant Agency and the project MSM 6046137306 of the Czech Ministry of Education.

References

[1] J. Kosek, F. Štěpánek, M. Marek. Modeling of transport and transformation processes in porous and multiphase bodies. *Adv. Chem. Eng.*, **30**, 137 (2005).
[2] I. Chorkendorff, J.W. Niemantsverdriet. *Concepts of Modern Catalysis and Kinetics*, Wiley-VCH, Weinheim (2003).
[3] G. Ertl. Heterogeneous catalysis on atomic scale. *J. Mol. Catal. A Chem.*, **182–183**, 5 (2002).
[4] P.M. Adler. The method of reconstructed porous media. *Curr. Top. Phys. Fluids*, **1**, 227 (1994).
[5] F. Štěpánek, M.A. Ansari. Computer simulation of granule microstructure formation. *Chem. Eng. Sci.*, **60**, 4019 (2005).
[6] M. Kohout, A.P. Collier, F. Štěpánek. Effective thermal conductivity of wet particle assemblies. *Int. J. Heat Mass Tran.*, **47**, 5565 (2004).

[7] F. Štěpánek, M. Marek, P.M. Adler. Modeling capillary condensation hysteresis cycles in reconstructed porous media. *AIChE J.*, **45**, 1901 (1999).
[8] F. Štěpánek, M. Marek, J. Hanika, P.M. Adler. Mesoscale modeling in multiphase catalysis. *Catal. Today*, **66**, 249 (2001).
[9] F.J. Keil. Modeling of phenomena within catalyst particles. *Chem. Eng. Sci.*, **51**, 1543 (1996).
[10] M.O. Coppens. Structuring catalyst nanoporosity. *Structured Catalysts and Reactors*, CRC Taylor and Francis, Boca Raton (2006).
[11] K. Ramanathan, V. Balakotaiah, D.H. West. Light-off criterion and transient analysis of catalytic monoliths. *Chem. Eng. Sci.*, **58**, 1381 (2003).
[12] R.E. Hayes, B. Liu, M. Votsmeier. Calculating effectiveness factors in non-uniform washcoat shapes. *Chem. Eng. Sci.*, **60**, 2037 (2005).
[13] P. Kočí, M. Kubíček, M. Marek. Modeling of TWC monolith converters with microkinetics and diffusion in the washcoat. *Ind. Eng. Chem. Res.*, **43**, 4503 (2004).
[14] P. Kočí, M. Kubíček, M. Marek. Periodic forcing of three-way catalyst with diffusion in the washcoat. *Catal. Today*, **98**, 345 (2004).
[15] P. Kočí, F. Štěpánek, M. Kubíček, M. Marek. Meso-scale modeling of CO oxidation in digitally reconstructed porous Pt/γ-Al_2O_3 catalyst. *Chem. Eng. Sci.*, **61**, 3240 (2006).
[16] A.P. Roberts. Morphology and thermal conductivity of model organic aerogels. *Phys. Rev. E*, **55**, 1286 (1997).
[17] B.E. Poling, J.M. Prausnitz, J.P. O'Connel. *The Properties of Gases and Liquids*, McGraw-Hill, New York (2001).
[18] F. Zhang, R.E. Hayes, S.T. Kolaczkowski. A new technique to measure the effective diffusivity in the washcoat of a monolith reactor. *Chem. Eng. Res. Des.*, **82(A4)**, 481 (2004).
[19] R.M. Heck, R.J. Farrauto. Automobile exhaust catalysts. *Appl. Catal. A: Gen.*, **221**, 443 (2001).
[20] J. Jirát, M. Kubíček, M. Marek. Adsorber-reactor systems for emission treatment from mobile sources. *Chem. Eng. Sci.*, **56**, 1597 (2001).
[21] J. Kašpar, P. Fornasiero, N. Hickey. Automotive catalytic converters: current status and some perspectives. *Catal. Today*, **77**, 419 (2003).
[22] R.H. Nibbelke, A.J. Nievergeld, J.H.B.J. Hoebink, G.B. Marin. Development of a transient kinetic model for the CO oxidation by O_2 over a Pt/Rh/CeO_2/γ-Al_2O_3 three-way catalyst. *Appl. Catal. B: Env.*, **19**, 245 (1998).
[23] J.M. Harmsen, J.H.B.J. Hoebink, J.C. Schouten. Acetylene and carbon monoxide oxidation over a Pt/Rh/CeO_2/γ-Al_2O_3 automotive exhaust gas catalyst: kinetic modeling of transient experiments. *Chem. Eng. Sci.*, **56**, 2019 (2001).